Influence of Particle Collisions on the Characteristics of H-like Ion Emission due to Charge Exchange Reactions with Fast Atoms

A.A. Korotkov

IPP III/142 Januar 1989

MAX-PLANCK-INSTITUT FÜR PLASMAPHYSIK

8046 GARCHING BEI MÜNCHEN

MAX-PLANCK-INSTITUT FÜR PLASMAPHYSIK

GARCHING BEI MÜNCHEN

Influence of Particle Collisions on the Characteristics of H-like Ion Emission due to Charge Exchange Reactions with Fast Atoms

A.A. Korotkov

IPP III/142 Januar 1989

Die nachstehende Arbeit wurde im Rahmen des Vertrages zwischen dem Max-Planck-Institut für Plasmaphysik und der Europäischen Atomgemeinschaft über die Zusammenarbeit auf dem Gebiete der Plasmaphysik durchgeführt.

Influence of Particle Collisions on the Characteristics of H-like Ion Emission due to Charge-Exchange Reactions with Fast Atoms

A.A. Korotkov

Abstract

The effective emission cross-sections of CVI (3434 A, 5291 A, 7717 A), NVII (3887 A, 5669 A, 7926 A), OVIII (2976 A, 4341 A, 6068 A) lines in charge-exchange reactions of nuclei with hydrogen atoms are calculated. The ground state and the first excited state of hydrogen are considered. The calculation takes into account the mixing of nl-levels due to collisions with plasma deuterons and electrons and Stark l-mixing in the Lorentz field ($\bar{V} \times \bar{B}$).

Calculation of the effective cross-sections with allowance for the atomic beam density distribution in the plasma allows one to determine the line intensities.

Finally, the influence of the fine structure and Zeeman splitting on the 2976 A OVII line profile is considered.

Contents:

* On leave from Ioffe Institute, Leningrad, USSR.

Part 1. Effective emission cross-sections of visible lines of the H-like ions CVI, NVII and OVIII in charge-exchange reactions and corresponding line intensities in ASDEX plasma due to beam heating.

I. Introduction

To use charge-exchange spectroscopy successfully, it is necessary to know the cross-sections for populating nlm-states in the charge-exchange reaction; the influence of an electric field ($\bar{V} \times \bar{B}$) and collisions with ions should also be taken into account /1/. The influence of collisional and Stark mixing becomes more important with increasing principal quantum number n. This is the case when optical lines are used.

In Ref. /2/ the MIXSTN code, which takes collisional mixing of l-states into account was used for calculating VUV line intensities resulting from charge-exchange reactions. It is there that the term effective cross-section was introduced, being defined as the line intensity per unit volume divided by the impurity concentration and hydrogen atom flux.

In the calculations now presented the MIXSTN code is used to obtain the effective cross-sections of visible lines of CVI, NVII, OVIII ions. The transitions with $n \leq 12$ are considered, and collisional and Stark l-mixing are taken into account. The latter is found to be significant for $n > 6$.

Unlike those of VUV lines, the intensities of visible lines are affected by charge-exchange reactions from excited levels of hydrogen. In this case initial nl-populations from theoretical models /3,4/ are used. Only the first excited state of hydrogen will be taken into account. The best model is determined by comparing the results of the calculations with the line intensities obtained in ASDEX /5/.

II. Initial nlm-population

1. Charge-exchange reaction with hydrogen in the ground state.

a) $E_H \leq 25$ keV

The most basic approach to the problem of nlm-population due to charge-exchange reactions at velocities $V \leq 1$ a.u. ($E_H \leq 25$ keV) is to solve close-coupling equations on a molecular or atomic basis. Comparison of the theoretical result /6/ for the $(C^{6+}H)$ system, which takes into account 33 states on a molecular basis, with experiment /7/ confirms its reliability for $n \leq 5$. For the $(O^{8+}H)$ system the results of similar calculations /8/ are used. For the $(N^{7+}H)$ system the results of calculations taking into account up to 46 states on an atomic basis /9/ are used. Moreover, results of similar calculations /10/ are used for all systems for $n \geq 6$ because they seem to be better confirmed by experiments /7/ than the results of the theory /11/ used in Ref. /1/. Nevertheless, the theoretical results used tend to underestimate nl-populations for $n \geq 8$ at $E_H \leq 10$ keV, but the contribution of charge-exchange from the excited hydrogen state is, as a rule, more important in this case (see next section).

b) $E_H = 50$ kev

Classical calculations taking into account over-barrier transitions are very useful at $V \geq 1$ a.u. Moreover, classical transitions already become dominant at $V > 1/n_o$ a.u. in the case of charge-exchange reactions with hydrogen in the excited state characterized by the principal quantum number n_o. For $E_H = 50$ keV and $n_o = 1$ classical calculations /12/ are used.

2. Charge exchange reactions with hydrogen in the excited state $n_o = 2$

Unlike $n_o = 1$, the case $n_o = 2$ is only investigated in a few papers /3,4/ and there are no experimental data available.

The analytical formula for the cross-section was suggested in /3/ on the basis of a decay model taking into account under-barrier transitions of electrons:

$$\sigma_{n_m \pm \nu}(\ell) = \sigma_{n_m} \frac{2\ell+1}{Z} \exp\left(-\ell(\ell+1)/Z\right) \exp\left(-\frac{3Z^5 V^2}{2 n_m^6 V^2}\right) \qquad (1)$$

where $\nu = 0,1,2,\ldots$, $n_m \approx n_0 Z^{0.75}$ is the most populated level, and Z is the nuclear charge number (see also /13/).

The decay model is valid at $V \leq 1/n_0$, i.e. just for the low energies considered. Better results are given by the classical model. Classical results for a few systems including $(B^{5+}H)$ and $(Ne^{10+}H)$ are given in /4/.

Theory forecasts that levels with principal quantum number from $n = n_0\sqrt{Z}$ up to $n = n_0 Z$ are predominantly populated. The most populated level n_m nearly coincides with the middle of the interval mentioned. Therefore, we have $n_m(n_0 = 2) =$ 8-9, 9-10 and 11 for the $(C^{6+}H)$, $(N^{7+}H)$, and $(O^{8+}H)$ systems, respectively.

In the calculations the n-distribution for the $(B^{5+}H)$ system /4/ was used for $(C^{6+}H)$ and $(N^{7+}H)$, but with some changes in it. The form of the distribution remained the same but it was centered at the most populated level n_m which was varied from 8 to 10 for the first system and from 9 to 11 for the second one. For the $(O^{8+}H)$ system, the results from $(Ne^{10+}H)$ were used with variations of n_m from 9 to 11.

The initial normalized l-population was approximated by

$$\begin{cases} \dfrac{3}{n} \dfrac{\ell^2+1.7\ell+1.1}{n^2+1.1n+1.2}, & n \leq n_m \\ \dfrac{3}{n_m+1} \dfrac{\ell^2+1.7\ell+1.1}{(n_m+1)^2+1.1(n_m+1)+1.2}, & n > n_m,\ \ell \leq n_m \\ 0, & n > n_m,\ \ell > n_m \end{cases} \qquad (2)$$

which reflects the main features of the classical l-population known in the $n_0 = 1$ case /12,13/.

3. m-population

All theoretical models at $V \leq 1$ a.u. predict that within a given l the $m = 0$ state will be predominantly populated /13/ (m refers to the z-component of the orbital angular momentum, if we take the z-axis in direction of the internuclear axis). The UDWA model predicts the same result at $V > 1$ a.u. as well. Therefore, if the beam is injected along the magnetic field $\bar{B}$ (when the internuclear axis coincides with magnetic field direction), the orbital angular momentum of the final ionic state is perpendicular to $\bar{B}$ and $m_j = \pm 1/2$ substates are only populated where m_j is the z-component of the total angular momentum. If injection is perpendicular to $\bar{B}$, the orbital angular momentum of the final ionic state can be arbitrary directed to $\bar{B}$ and all possible m_j substates are populated. In other words, in the first case the $j = l \pm 1/2$ states will be equally populated because each of them contains an equal number of the $m_j = \pm 1/2$ substates. In the second case, the $j = l \pm 1/2$ states will be populated according to the number of the m_j substates, i.e. statistically. Both of the distributions were used in the calculations.

Furthermore, we shall be interested in the intensities of the $(n \rightarrow n')$ lines according to transitions between states characterized by principle quantum number only, i.e. we are not interested in the final j' m_j' states. Since the total probability of all transitions from a fixed state $(n\ l\ j\ m_j)$ to all states with fixed n' l' (but all possible values of j' m_j') is independent of the total angular momentum j and magnetic quantum number m_j of the initial state /15/, the features of the j-population within a given l very weakly affect the line intensities considered and hence the effective cross-sections.

III. Treatment in the MIXSTN code

1. The MIXSTN code solves a 143-equation system derived from a collisional-radiative model for time-integrated relative populations N_i:

$$\left(A_i + \sum_{\alpha,K} \langle \sigma v \rangle_{\alpha,iK} n_{p_\alpha} + \sum_K u_{St\,iK}\, \delta(\Delta E_{iK})\right) N_i - \sum_K \left(u_{St_{Ki}}\, \delta(\Delta E_{iK}) + A_{Ki} + \sum_\alpha \langle \sigma v \rangle_{\alpha,Ki} n_{p_\alpha}\right) N_K = \chi_i \qquad (3)$$

$$i, K \equiv \{ n \ell j \}, \quad n \leq 12$$

A_{ki} - probability of radiative transition from k to state i, $A_i = \sum_K A_{iK}$, $\langle 6v \rangle_\alpha$ - excitation rate coefficient (α = 1, 2 for deuterons and electrons, respectively), u_{St} - effective frequency of Stark mixing, $n_{p\alpha}$ - deuteron or electron density, which are considered to be equal, χ_i - initial relative population of i state due to charge-exchange reaction:

$$\chi_i = \left(\sigma_{cx_i}(n_o=1) + \xi\, \sigma_{cx_i}(n_o=2)\right) / \sigma_{cx_{tot}} \qquad (4)$$

$\sigma_{cx_i}(n_o = 1)$ - cross-section of charge-exchange reaction from hydrogen ground state to ionic state i, σ_{cx} (n_0 = 2) - the same for the first excited hydrogen state, $\sigma_{cx_{tot}}$ - total charge-exchange cross-section,
ξ - relative population of the first excited hydrogen state, which is calculated from system (3) on the assumptions $N_1 = 1$ and $\chi_i(n \geq 2) = 0$ (see Part 2).

The effective emission cross-section of the $n_2 \to n_1$ line, $\sigma_{eff}(n_2 \to n_1)$, is determined as

$$\sigma_{eff}(n_2 \to n_1) = \sigma_{cx_{tot}} \sum_{i,K} A_{iK} N_i \qquad (5)$$

where all dipole transitions contributing to $n_2 \to n_1$ transition are taken into account.

With σ_{eff} the line intensity can be calculated from

$$\mathcal{J} = \Phi n_z \sigma_{eff} \qquad [cm^{-3} \cdot s^{-1}] \tag{6}$$

Φ - hydrogen atom flux, n_z - nuclear density of the impurity.

2. Energetic level structure of H-like ions in a plasma with magnetic field

For the ASDEX magnetic field (= 20 kG) the energetic gaps between levels with different j are determined by fine splitting ΔE_{FS} up to $n \leq 7$:

$$\Delta E_{FS} = 7.2 \cdot 10^{-4} \frac{Z^4}{n^3} \left(\frac{3}{4n} - \frac{1}{j+1/2} \right) \quad [eV] \tag{7}$$

For $n > 7$ Zeeman splitting becomes comparable to ΔE_{FS} for the largest j. In this case for arbitrary relations between fine and Zeeman splitting the energetic splitting is /16/:

$$\Delta E = \Delta E_{FS} \left(\gamma m_j \pm \frac{1}{2} \sqrt{1 + \gamma \frac{4 m_j}{2l+1} + \gamma^2} \right) \tag{8}$$

$$\gamma = \mu_0 B / \Delta E_{FS}, \quad \mu_0 = e\hbar/2mc$$

The Stark effect in the field $(\bar{V} \times \bar{B})$ for T = 1 keV degenerates some states with equal j for $n > 7$:

$$\Delta E_{st} = 4 \cdot 10^{-9} \frac{n m_j}{Z} \frac{\sqrt{n^2 - (j+1/2)^2}}{j(j+1)} \mathcal{E} \quad [eV] \tag{9}$$

$$\mathcal{E} = 13.2 \sqrt{T/A}\, B \quad [V \cdot cm^{-1}]$$

T in eV, B in kG, A - atomic weight of ion considered. For s-states the Lamb shift is significant:

$$\Delta E_L = 4.5 \cdot 10^{-6} \frac{Z^4}{n^3} \left(16.5 + 2 \ln (137/Z) \right) \quad [eV] \tag{10}$$

s-states are of no great practical importance for visible lines of impurity ions but have significance for the resonance lines and the population of the excited hydrogen states (especially due to 2s-state).

3. Collisional mixing

a) l-mixing for a given n is determined by collisions with deuterons, transitions between n levels by collisions with electrons and deuterons.

The MIXSTN code only takes dipole transitions into account ($\Delta j = 0, \pm 1$, $\Delta m_j = 0, \pm 1$).

For transitions between non-degenerate l-states of the same n the code uses cross-sections from the close-coupling theory of two states /17, 2/ (atomic units are used):

$$\langle \sigma V \rangle_{ik} = \frac{2\sqrt{2\pi}}{3} |r_{ik}|^2 \sqrt{\frac{\mu}{T}} \int_{\Delta E/T}^{\infty} \exp\left(-\left(2\sqrt{\frac{\alpha}{\varepsilon}} + \varepsilon\right)\right) I_2\left(\frac{\alpha}{\varepsilon}\right) d\varepsilon \qquad (11)$$

$\varepsilon = \mu V^2/2T$, $\alpha = |r_{ik}| \Delta E \mu / 2\sqrt{3} T$, $I_2\left(\frac{\alpha}{\varepsilon}\right)$ -function is tabulated in /17/, μ - reduced mass, ΔE - energy of the transition, $/r_{ik}/$ - dipole matrix element averaged over initial m_j states and summed over the final states:

$$|r_{ik}|^2 = \begin{cases} \frac{g}{16 j(j+1)} \frac{n^2}{Z^2} \left(n^2 - (\ell+1)^2\right), & j \to j, \ \ell \to \ell+1 \\ \frac{g}{4} \frac{2j+3}{4(j+1)} \frac{n^2}{Z^2} \left(n^2 - (\ell+1)^2\right), & j \to j+1, \ \ell \to \ell+1 \end{cases} \qquad (12)$$

For $l \to l-1$ transitions $|r_{ki}|^2 = \frac{2j+1}{2j'+1} |r_{ik}|^2$ and l is to be changed by (l - 1).

Multiplet averaging does not greatly change the cross-sections, because for $\Delta n = 0$ $E >> \Delta E\mu$ and cross-sections depend on ΔE very weakly $\left(I_2\left(\frac{\alpha}{\varepsilon}\right) \sim \ln(\Delta E)\right)$. For $\Delta n \neq 0$ transitions ΔE strongly exceeds the energetic width of multiplets and therefore the averaging mentioned is again a good approximation.

b) For collisional transitions between degenerated states the code uses the cross-section of Pengelly and Seaton, taking into account a cutoff impact paramater equal to the Debye radius /1/:

$$\langle \sigma v \rangle_{ik} = 9.2 \cdot 10^{-8} \lambda \sqrt{\frac{M}{T}} \left(21.35 + \log\left(T^2/\mu \lambda n_p\right)\right) \quad [cm^3 \cdot s^{-1}]$$
$$\lambda = \frac{6n^2}{Z}\left(n^2 - \ell^2 - \ell - 1\right) \qquad (13)$$

μ in a.u., T in eV, n_p in cm^{-3}.

c) For transitions between n-states due to collisions with deuterons formula (11), normalized to experimental hydrogen results /18/, at $\alpha/\varepsilon > 10^{-3}$, is used. For electrons van Regemorter's formula is used:

$$\langle \sigma v \rangle_{n_i n_k} = 1.6 \cdot 10^{-5} G_{n_i n_k} f_{n_i n_k} \frac{\exp(-\Delta E/T)}{\Delta E \sqrt{T}} \quad [cm^3 \cdot s^{-1}] \qquad (14)$$

ΔE and T in eV, $n_k > n_i$.

Gaunt factor:

$$G_{n_i n_k} = 0.19\left[1 + 0.9\left[1 + 0.05 n_k (n_k - n_i)\left[1 + (1 - 2/Z)\frac{\Delta E}{T}\right]\right]\right] \exp\left(\frac{\Delta E}{T}\right) E_1\left(\frac{\Delta E}{T}\right)$$

$f_{n_k n_i}$ - oscillator strenght,

d) For Stark mixing of the degenerated states the MIXSTN code uses an effective frequency:

$$\mathcal{U}_{St_{ik}} = \Delta E_{St}/\hbar \quad , \quad \mathcal{U}_{St_{ki}} = \frac{g_i}{g_k} \mathcal{U}_{St_{ik}} \quad , \quad k > i \qquad (15)$$

e) For calculation of ionization rate coefficients for ionic and hydrogen states Lotz's formula is used.

IV. Results and discussion

Figures 1 - 3 show the effective cross-sections as functions of the plasma density n_p for hydrogen beams with energies E_H = 10, 25 and 50 keV. Figure 1 represents also cross-sections resulting from charge-exchange of the hydrogen ground state to demonstrate the effect of excited atoms in the beam. This effect is most pronounced for the longest wavelengths at $E_H \leq 25$ keV. The variation of the cross-sections with plasma density at $E_H \leq 25$ keV mostly reflects an increasing population of the excited hydrogen state at $n_p < 10^{15}$ cm^{-3}. Then this population is constant but the collisional lifetime of the excited ionic states becomes comparable to the radiative one, therefore cross-sections are nearly constant or even reduced.

Cross-sections for the shortest wavelengths CVI (3434 A), NVII (3887 A), OVIII (2976 A) are nearly independent of the plasma density at $E_H \geq 25$ keV and $n_p < 10^{15}$ cm^{-3}. These lines are therefore very useful for impurity concentration measurements. On the other hand, the cross-sections for the longest wavelengths resulting from charge-exchange of the excited hydrogen state become comparable with others at $n_p \geq 10^{13}$ cm^{-3} for all hydrogen energies considered.

Figures 4 - 6 present the values of the effective cross-sections multiplied by the hydrogen velocity (excitation rate coefficients). Excitation rate coefficients from Ref. /1/ not taking into account charge-exchange from the excited hydrogen state are also shown. The most pronounced discrepancies between the data exist at low hydrogen energy $E_H < 25$ keV owing to charge-exchange from the excited hydrogen state. Moreover, the behaviour of the coefficients as functions of the plasma density are different. According to Ref. /1/, "yrast" transition rate coefficients decrease with increasing plasma density because the theory gives an initial l-population exceeding the statistical one for large l. But as shown in Figures 1-3, the increasing excited hydrogen state population with plasma density results in opposite behaviour of the cross-sections at $n_p < 10^{15}$ cm^{-3}, $E_H \leq 25$ keV due to charge-exchange from this hydrogen state.

Figure 7 shows the effective cross-sections of carbon as functions of the plasma density to demonstrate the influence of collisional mixing on line intensities. For this purpose the relative population of the hydrogen excited state was fixed at $\xi = 3.4 \cdot 10^{-3}$ and is assumed to be independent of the plasma density. The cross-section for the shortest wavelength CVI (3434 A) at 10 keV shows the most sensitive variations with density. The influence of the plasma density on the cross-sections disappears at $n_p = n_p^* \geq 10^{14}$ cm^{-3} because of the statistical l-population that takes place for $n \geq 7$ levels of the CVI ion. The minimum value of n_p^* obtained by assuming the radiative and collisional lifetimes of the levels to be equal /1/ is nearly one order of magnitude lower. The results obtained reflect that for the statistical l-population, however, it is necessary that the radiative lifetime substantially exceeds the collisional one.

The cross-sections reveal the greatest variations with the plasma density for $E_H = 10$ keV because in this case charge-exchange from the excited hydrogen state is the most efficient. In this case the population of the highest l-levels strongly exceeds the statistical one (see Part 1, Sect. II.2.). Collisions result in a statistical population and therefore, the cross-sections for the "yrast" transitions decrease (see also Fig. 8).

Figure 8 represents effective cross-sections of carbon obtained from different theories at $\xi = 3.4 \cdot 10^{-3}$ to demonstrate the significance of the initial nl-population. As was mentioned in Part 1, Sect. II.2 in the case of calculations taking into account charge-exchange from the excited hydrogen state, the forms of the n-distributions from Ref. /4/ were used but they were centered at the most populated level n_m which was varied. The influence of these variations is also shown.

The theory /11/ as used in Ref. /1/ gives, as a rule, higher values of the cross-section at $E_H \geq 25$ keV (in the absence of l-mixing and charge-exchange from the excited hydrogen state) because the l-population strongly exceeds the statistical one for large l. On the other hand, the decay model underestimates the cross-sections because it considers underbarrier transitions only. Moreover, it gives the opposite dependence of the cross-section on the plasma density because the l-population for large l is underestimated.

As was mentioned above, the cross-sections are determined by charge-exchange from the excited hydrogen state at a beam energy of 10 keV. This is also the case for 25 keV for transitions from $n \geq 8$ levels. The contribution of charge-exchange from the excited hydrogen state becomes insignificant for a beam energy of 50 keV. The uncertainty resulting from the nl-distribution therefore becomes weaker when the beam energy increases.

The best model of nl-population in the case of charge-exchange from the excited hydrogen state was chosen by calculating the ratios of the CVI (7717 A/5291 A) and OVIII (6068 A/2976 A) lines at different shifts of the n-distributions from Ref. /4/ as was mentioned above and comparing them with experimental results obtained on ASDEX /5/ (Fig. 9). The intensities of the CVI (3434 A) and OVIII (4341 A) lines from this experiment were not used because of line blending with the OVI and H_γ lines, respectively.

It can be seen that l-mixing does not affect the choice of the nl-distribution model. The calculations show that the best nl-distribution models correspond to the principal quantum numbers of the most populated states n_m = 8 - 9 for CVI and n_m = 10 for OVIII. Model /4/ also gives good results for the ratio NVII (7926 A/5669 A) for n_m = 9. But the intensity of the NVII (3887 A) line cannot be explained by variation of the nl-population in the classical theory /4/. Figure 9 also shows that charge-exchange from the excited hydrogen state must be taken into account to explain the oxygen line ratio.

The best nl-population models were used for obtaining the results represented in Figs. 1 - 6.

Figure 10 represents the line intensities under the conditions of the ASDEX experiments /5/. In the calculations the distribution of the beam density in the plasma for all beam energy fractions was treated with the NEUDEN code /16/. The line intensities integrated along the line of sight are not so sensitive as the cross-sections to models of the nl-population due to charge-exchange from the excited hydrogen state. The contribution of charge-exchange from the excited hydrogen state n_0 = 2 is approximately 50% for CVI (7717 A, 5291 A), NVII (7926 A, 5669 A), OVIII (6068 A, 4341 A) and 20% for CVI (3434 A), NVII (3887 A), OVIII (2976 A) lines.

The influence of collisional mixing does not exceed 30%. There are two reasons for this: first, collisional mixing is most noticeable for the $E_H/3$ fraction of the heating beam, which is strongly attenuated in the plasma; second, summing the intensities from the 20 keV and 41 keV fractions of the beam partly compensates the effect of collisional mixing. It can be seen from Figs. 7, 8 that collisional mixing decreases the cross-sections for a beam energy of 25 keV and increases them for 50 keV.

V. Conclusions

The most reliable measurement of the impurity concentration using the ASDEX heating beams is predicted for the CVI (3434 A), NVII (3887 A), OVIII (2976 A) lines (provided background radiation allows them to be clearly observed). The intensities of these lines are most insensitive to charge-exchange from excited states of hydrogen atoms (contributing only ≈20% in this case).

Application of other lines for concentration measurements would require the amount of excited atoms in the heating beam to be known. Moreover, the details of the nl-population can be important for the longest wavelengths. These lines should therefore not be used for density measurements, but they may be interesting for ion temperature measurements because their effective cross-sections become comparable with the cross-sections of the strongest lines at $n_p \geq 10^{13}$ cm^{-3} owing to charge-exchange from the excited hydrogen state. These lines could also prove useful for testing charge-exchange theories.

All results presented were obtained for T = 1 keV and B = 22 kG. Nevertheless, these results can be applied for the ranges $10^2 < T < 10^4$ eV and 10 < B < 30 kG because excitation cross-sections very weakly depend on ΔE and $\Delta E \ll T$ for all important transitions.

Part 2. Population of excited hydrogen states in the ASDEX heating beam.

Ratios of the excited hydrogen state populations ($n \leq 5$) to the ground state n = 1 were calculated for hydrogen beam energies of E_H = 10, 20.5, 41 keV in a wide region of plasma parameters ($1 \cdot 10^{13}$ cm^{-3} < N < $1 \cdot 10^{16}$ cm^{-3}, 0.1 < T < 10 keV). The intensities of Lα (1216 A), Lβ (1026 A), Hα (6565 A), Hβ (4863 A) lines were determined.

As was found in Part 1 for the calculations of the effective emission cross-sections of visible ion lines produced by charge-exchange reactions of atoms with plasma ions at $E_H \leq 25$ keV, it is necessary to take into account the fraction of excited atoms in the beam. Moreover, the emission of excited hydrogen atoms in the beam can be used for absolute or relative calibration of the spectrometers used. The lines of the beam can generally be well distinguished from other lines due to large Doppler shifts.

Calculations of the equilibrium hydrogen state populations were made by means of the MIXSTN code (see Part 1, Sect. III). The equilibrium population of the excited states is reached after times close to the radiative lifetimes of the states. These times are $\tau_r \leqq 10^{-7}$ s for $n \leqq 5$ (the 2 s state has a lifetime nearly equal to that of the 2 p state owing to strong Stark mixing in the Lorentz field). Therefore, the length of the beam path in the plasma l_{eq} necessary to reach the equilibrium excited-state population is equal to $(V \cdot \tau_r)$.

Figure 11 represents the value l_{eq} for the most energetic beam component as a function of the principle quantum number of the states. The equilibrium population for $n \leqq 3$ is already reached at the plasma edge ($l_{eq} \leqq 3$ cm); for $n = 4$ and $n = 5$ we find $l_{eq} \approx 10$ cm. Use of the MIXSTN code is valid at $l > l_{eq}$.

Figure 12 shows the relative population ξ of the states as a function of the plasma density for 20.5 keV beam energy. Stark l-mixing results in a statistical l-population independently of the plasma density. Collisional l-mixing itself results in a statistical l-population $n \leqq 3$ only at $n_p \approx 10^{14}$ cm^{-3}.

Owing to the statistical l-population the ξ values increase because the average radiative lifetime is larger than that of the np-states. This effect is most pronounced for the highest n-states.

Figure 13 represents the population of the hydrogen states as a function of the beam energy. The increasing ξ with beam energy results from excitation of the beam by deuterons.

The values ξ shown in Fig. 12 depend weakly on the plasma temperature. These values can therefore be used for the wide temperature range mentioned.

Figure 14 shows the dependence of the hydrogen line intensities per hydrogen atom on the plasma density at $E_H = 20.5$ keV.

Accuracy of the results.

Stark l-mixing in the Lorentz field ($\bar{V} \times \bar{B}$) definitely results in a statistical population of the l-sublevels within the n-states at the hydrogen beam energy considered and B = 20 kG. The accuracy of the results obtained is therefore determind by the accuracy of the collisional cross-sections used for transitions

between states of different n. The comparison of the electron and deuteron excitation rates for different energy fractions of the beam shows that electrons determine the beam excitation at E_H = 10 and 20.5 keV but contributions of electrons and deuterons are comparable at E_H = 41 keV.
The electron cross-sections were described by van Regemorter's formula. The comparison of van Regemorter's cross-section with experimental results and results of more exact calculations represented in Ref. /17/ shows that the accuracy of these cross-sections is better than 6% for the 1s-2p transition and about 20% for n = 2 → n = 3 → n = 4 transitions (the 1s-2s transition cannot be described by van Regemorter's formula but its contribution is only 10% in comparison with the 1s-2p transition).

The exciation of hydrogen by deuteron was described by the formula (11) normalized to the experimental results /18/ for n = 1 - n = 2 transition. It has 20% accuracy at E = 41 keV for the other transitions from the ground state of hydrogen that can be confirmed by comparison with more precise theoretical results /20/.

As a consequence, the uncertainty of the relative populations of the n = 2 level and L_α intensity is less than for the populations n ≥ 3, and for the corresponding intensities we estimate accuracies of ≤ 40%.

Part 3. Influence of the fine structure and Zeeman splitting on visible line profiles

The profile of the 2976 A OVIII line (n = 8 → 7) was calculated, taking into account the fine and Zeeman energy structures of the ion for a magnetic field of 22 kG by means of the MIXSTN code, which calculates the population of ionic nlj-levels and intensities of the fine-structure components. The total line profiles were obtained from a superposition of Gaussian line shapes centered at the position of the fine-structure components.

The main transitions contributing to the intensity that are taken into account are $K_{15/2} \to i_{13/2}$, $K_{13/2} \to i_{11/2}$, $i_{13/2} \to h_{11/2}$, $i_{11/2} \to h_{9/2}$, $h_{11/2} \to g_{9/2}$, $h_{9/2} \to g_{7/2}$, $g_{9/2} \to f_{7/2}$, $g_{7/2} \to f_{5/2}$, $f_{7/2} \to d_{5/2}$.

Stark mixing in the Lorentz field only affects the $s_{1/2}$ and $p_{1/2}$ levels in this case and therefore does not influence the lines considered.

At plasma temperature of 1 keV Zeeman splitting is negligible compared to Doppler broadnening and must not be taken into account. At low temperatues (such as 50 eV) Zeeman splitting of the l-states considered can be as much as 10% in comparison with the Doppler width. To assess the magnitude of this effect the widths of the fine-structure components in the absence of motional broadening were assumed to be equal to the separation between extreme Zeeman components.

The comparison of the separations beween Zeeman terms of the neighbouring l-states with the same j and m_j values (ΔE_{Zeeman}) with Stark shifts of these terms (for n = 8) in the Lorentz field (ΔE_{St}) gives $\Delta E_{St}/\Delta E_{Zeeman}$ = 0.5, 0.3, 0.2 for j = 1/2, 3/2, 5/2 accordingly. This means that Stark mixing only affects the $s_{1/2}$ and $p_{1/2}$ levels and therefore does not influence the lines considered.

The line profiles and relative intensities of the strongest fine-structure components for different plasma densities are presented in Figs. 15, 16. As was metioned in Part 1, the population of the highest ionic l-levels due to charge-exchange strongly exceeds the statistical one. (at least for $E_H \leq 25$ keV). Collisions resulting in statistical l-population give more uniform intensity distribution of the fine-structure components. Therefore, when the plasma density increases the lines become wider until statistical l-population becomes important.

The relative difference of the temperature determined on the assumption of just Doppler broadening to the real temperature is shown in Fig. 17 as a function of the plasma density. The results from Ref. /1/ on the assumption of a statistical l-distribution are also presented. A statistical l-distribution for the n = 8 level of the OVIII ion was found to exist at $n_p \geq 10^{14}$ cm^{-3} (see Part 1). Rather good agreement of the data at these densities is found.

Acknowledgements

The author wishes to thank Dr. G. Fussmann for a critical reading of the manuscript and great help in preparing the final version of this paper.

1. R.J. Fonck, D.S. Darrow, K.P. Jaehnig, Phys. Rev. A29, 3288, (1984).
2. A.A. Korotkov, A.N. Zinoviev, Sov. Plasma Phys., 14, N 12, (1988).
3. E.L. Duman, L.I. Men'shikov, B.M. Smirnov, Sov. Phys.-JETP, 49, 260, (1979).
4. R.E. Olson, J. Phys B 13, 483, (1980).
5. P.G. Carolan et al., Phys.Rev. A 35, N 8, 3454-3471, (1987).
6. T.A. Green, E.J. Shipsey, J.C. Browne, Phys.Rev. A 25, N 3, 1364, (1982).
7. R. Hoekstra et al., Z. Physik D8, 57 (1988).
8. E.J. Shipsey, T.A. Green, J.C. Browne, Phys.Rev. A 27, N 2, 821, (1983).
9. W. Fritsch, C.D. Lin, Phys. Rev. A 29, N 6, 3039, (1984).
10. W. Fritsch, Phys. Rev. A 30, N 6, 3324, (1984).
11. H. Ryufuku, Japan Atomic Energy Research Institute Report JAERI-82031, 1982.
12. R.E. Olson, Phys. Rev. A 24, N 4, 1726-1733, (1981).
13. R.K. Janev, Physica Scripta T3, 208, (1983).
14. H. Ryufuku, T. Watanabe, Phys. Rev. A 20, N 5, 1828, (1979).
15. H.A. Bethe, E.E. Salpeter, "Quantum mechanics of one and two-electron atoms", Springer-Verlag, Berlin-Göttingen-Heidelberg, 1957, p. 272.
16. Ibid. p. 211.
17. L.A. Vanstein, I.I. Sobelman, E.A. Yukov "Excitation of atoms and broadening of spectral lines", Moscow, "Nauka", 1973.
18. J.T. Park, J.E. Aldag, J.M. George, Phys. Rev. Lett. 34, 1253 (1975).
19. F.P. Penningsfeld, IPP Report 4/229, Max-Planck-Institut für Plasmaphysik, 1986.
20. R. Shakeshaft, Phys. Rev. A 18, N 5, 1930 (1978).

Fig. 1 Effective emission cross-sections vs. plasma density for CVI lines:1- 3434 A, 2- 5291 A, 3- 7717 A;
Solid lines - taking into account charge-exchange from the ground and the first excited hydrogen states, dashed lines - without charge-exchange from the excited hydrogen state.

Fig. 2 The same as Fig. 1 but for the NVII lines: 1- 3887 A, 2- 5669 A, 3- 7926 A.

Fig. 3 The same as Fig. 1 but for the OVIII lines: 1- 2976 A, 2- 4341 A, 3- 6068 A.

Figs. 4,5,6 Excitation rate coefficients for CVI, NVII, OVIII lines vs. hydrogen beam energy and plasma density:
1- $n_p = 2 \cdot 10^{11}$ cm^{-3}, 2- $n_p = 5 \cdot 10^{13}$ cm^{-3}, 3- $n_p = 5 \cdot 10^{14}$ cm^{-3}, 4 and 5 from Ref. /1/ without l-mixing and with full l-mixing, respectively, and without charge-exchange from the excited hydrogen state.

Fig. 7 Effective cross-sections vs. plasma density for CVI lines 1- 3434 A, 2- 5291 A, 3- 7717 A at fixed excited hydrogen state population $\xi = 3.4 \cdot 10^{-3}$. The H-beam energy in keV is given in brackets.

Fig. 8 Effective cross-sections for CVI lines obtained from different models of nl-population:

O—O - taking into account nl-mixing with different initial nl-population characterized by the most populated state n_m values given near curves due to charge-exchange from the excited hydrogen state.

O--O - the same without mixing

●—● - with nl-mixing but for charge-exchange from ground state of hydrogen only

□,■ - decay theory /3/ without and with mixing

◊,◆ - the same but for UDWA theory /11/.

Fig. 9 Comparison of experimental and calculated line ratios η:
1- experiment /5/,
2,3- calculations with and without l-mixing respectively,
4- taking into account charge-exchange from the hydrogen ground state only,
n_m - the maximum populated level by charge-exchange from excited hydrogen state at which theoretical n-distributions from Ref. /4/ were centered.

Fig. 10 Calculated relative line intensities integrated along the line of sight J obtained for ASDEX conditions:
solid lines - with nl-mixing taken into account,
dashed lines - without nl-mixing,
open circles - without taking into account charge-exchange from the hydrogen excited state.

Fig. 11 Length of the beam in plasma for reaching the equilibrium excited hydrogen state population as a function of principal quantum number (E_H = 41 keV).

Fig. 12 Population of n-hydrogen states ξ normalized to n = 1 state population. Values near curves denote principal quantum numbers.

Fig. 13 Population of the excited hydrogen states characterized by principal quantum number n vs. beam energy for different plasma densities:
1 - $n_p = 10^{13}$ cm^{-3},
2 - $n_p = 10^{14}$ cm^{-3},
3 - $n_p = 10^{15}$ cm^{-3}.
Each population is divided by that for E_H = 20.5 keV.

Fig. 14 Intensities of hydrogen lines per unit hydrogen beam density vs. plasma density at E_H = 20.5 keV: 1 - L_α, 2 - L_β, 3 - H_α, 4 - H_β.

Fig. 15 Line profiles for the OVIII (n = 8 - 7) transition at T_i = 50 eV, E_H = 10 keV, B = 22 kG:
—— - without taking into account any energy splitting
×——× - $n_p = 1 \cdot 10^{12}$ cm^{-3} with fine and Zeeman structures
●——● - $n_p = 1 \cdot 10^{13}$ cm^{-3} taken into account
+——+ - $n_p = 1 \cdot 10^{14}$ cm^{-3}
○——○ - $n_p = 1 \cdot 10^{15}$ cm^{-3}
The relative intensities of the line components are represented for cases:
—— - $n_p = 1 \cdot 10^{12}$ cm^{-3}
– – – - $n_p = 1 \cdot 10^{14}$ cm^{-3}
The separation between extreme Zeeman terms are also shown as the widths of the fine-structure components.

Fig. 16 The same as Fig. 15 but for higher plasma temperature T = 1000 eV and beam energy E_H = 25 keV, B = 22 kG:

1 - without taking into account the energy structure

2 - $n_p = 2 \cdot 10^{11}$ cm^{-3} with fine and Zeeman energy structures

3 - $n_p = 1 \cdot 10^{14}$ cm^{-3} taken into account

4 - $n_p = 1 \cdot 10^{16}$ cm^{-3}

The relative intensities of the main line components are shown for the $n_p = 2 \cdot 10^{11}$ cm^{-3} case.

Fig. 17 Ion temperature correction factors due to fine structure and Zeeman splitting vs. plasma density for OVIII with excitation by E_H = 10 keV (at T_i = 50 eV) and E_H = 25 keV (at T_i = 1 keV) hydrogen beam (B = 22 kG),

■, □ - from Ref. /1/ at T = 100 eV and T = 1000 eV for complete l-mixing.

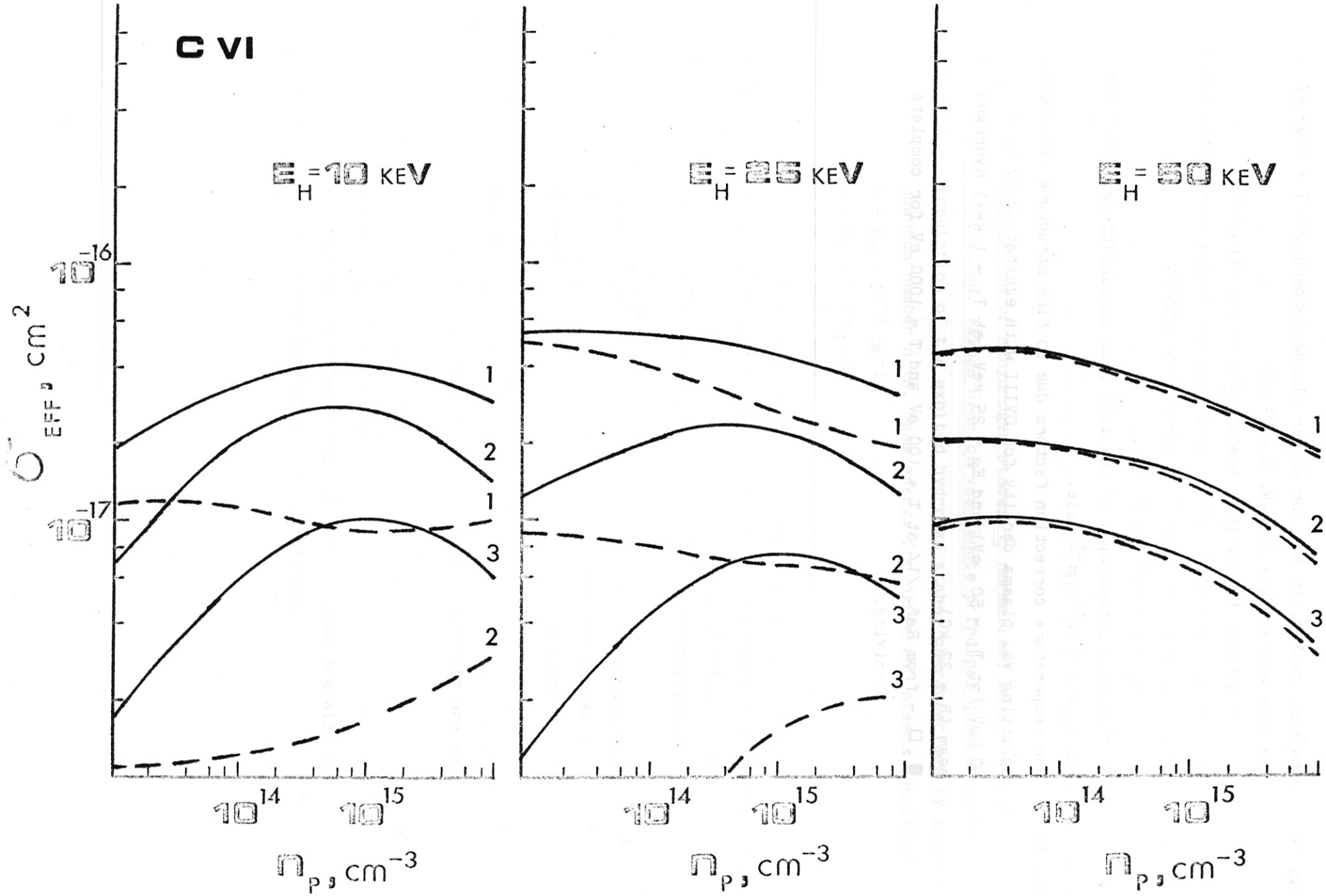
C VI
E_H = 10 KEV
E_H = 25 KEV
E_H = 50 KEV
σ_EFF, cm^2
10^-16
10^-17
1
2
3
10^14
10^15
n_p, cm^-3

Fig.1

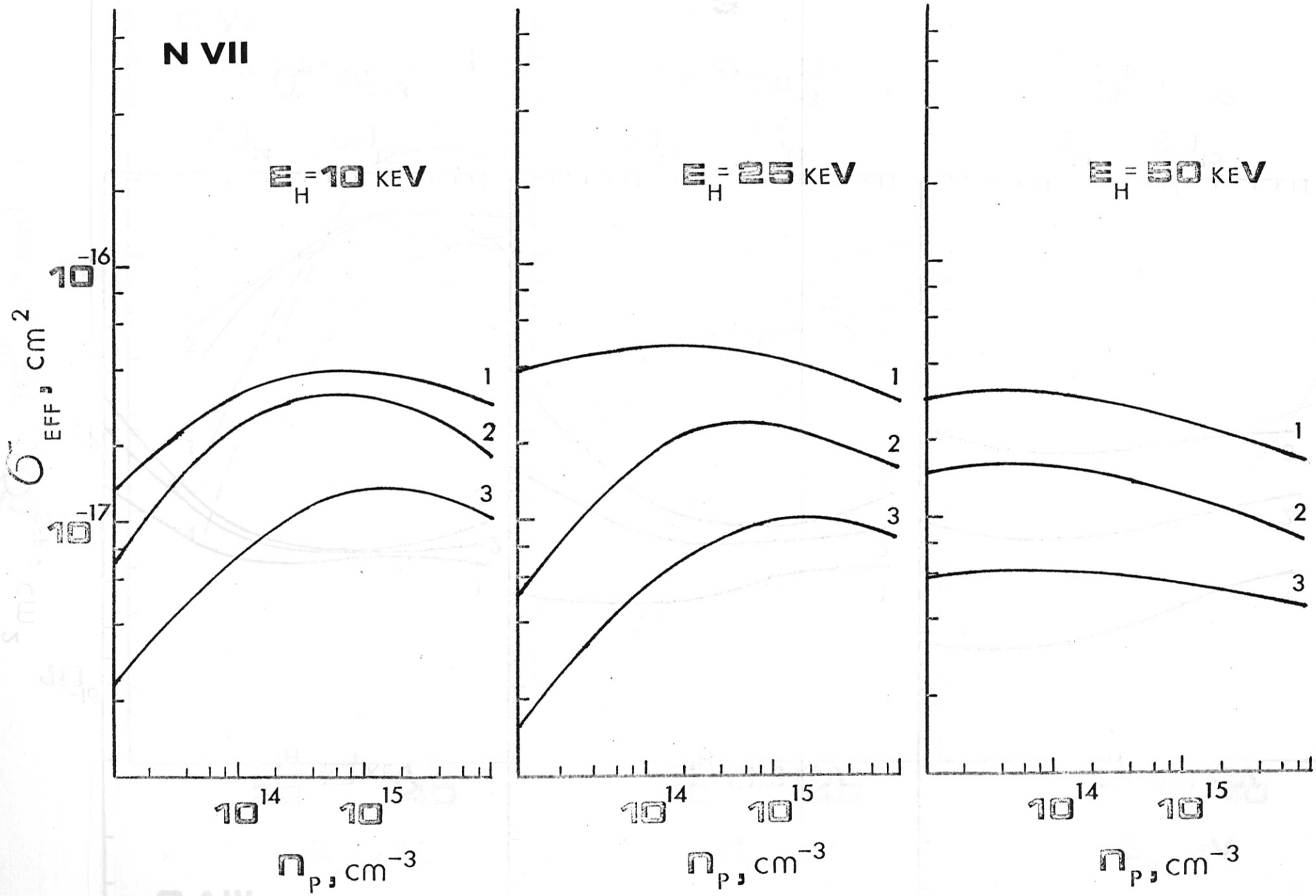
N VII
E_H = 10 KEV
E_H = 25 KEV
E_H = 50 KEV
σ_{EFF}, cm^2
10^{-16}
10^{-17}
1
2
3
10^{14}
10^{15}
n_p, cm^{-3}

Fig. 2

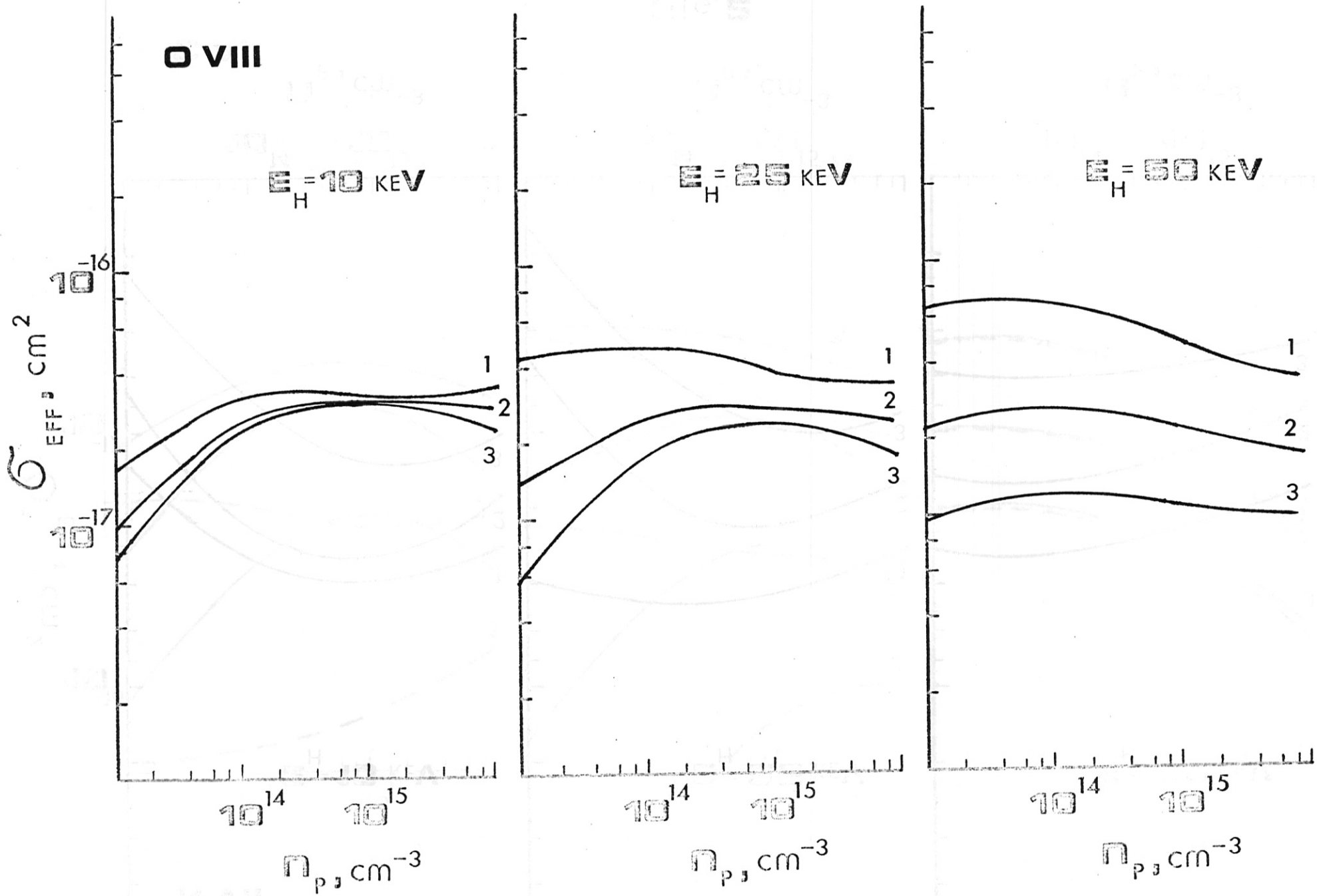
O VIII
E_H = 10 KeV
E_H = 25 KeV
E_H = 50 KeV
σ_{EFF}, cm^2
10^{-16}
10^{-17}
1
2
3
10^{14}
10^{15}
n_p, cm^{-3}

Fig. 3

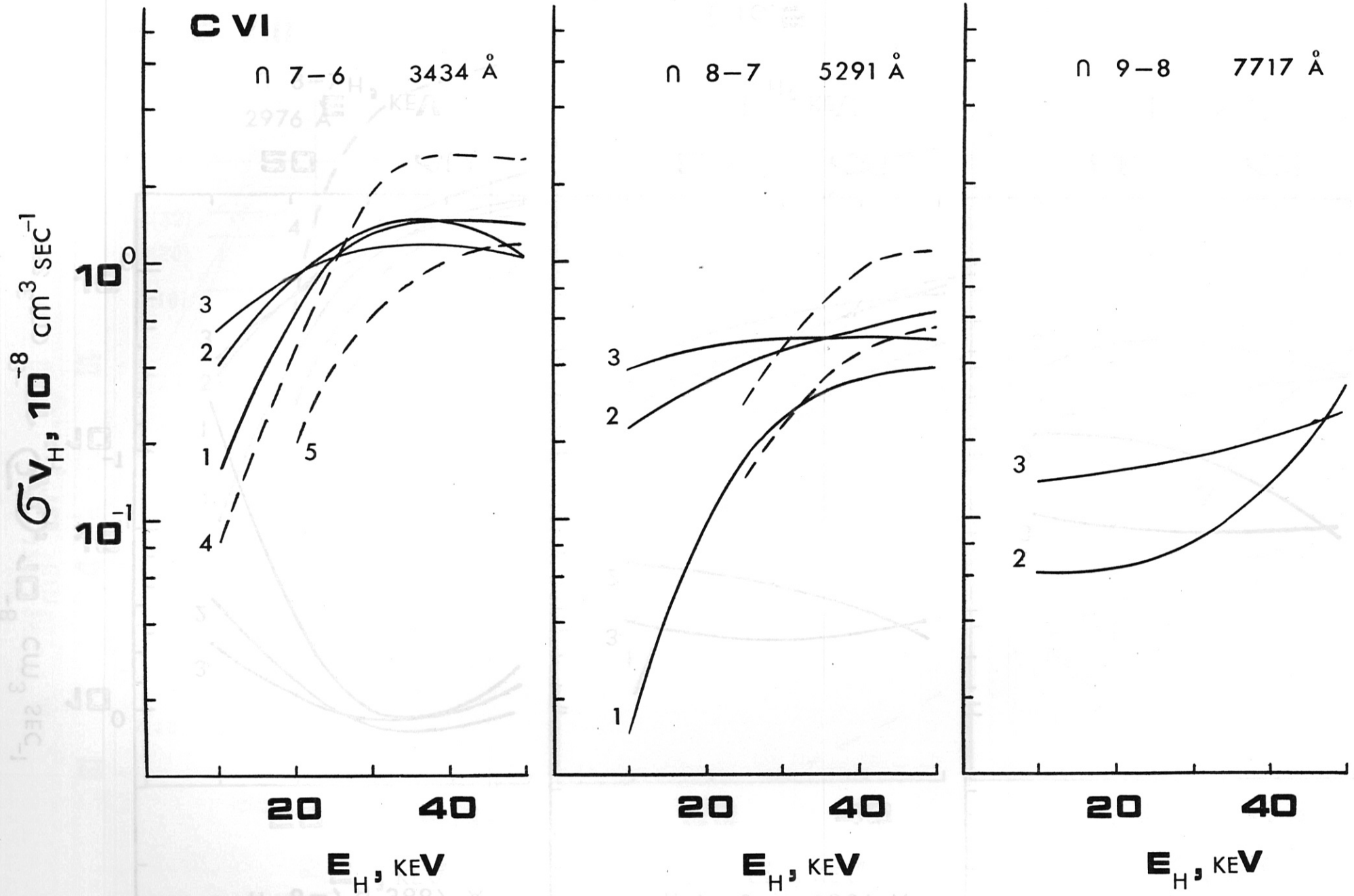
C VI
n 7–6 3434 Å
n 8–7 5291 Å
n 9–8 7717 Å
σv_H, 10^{-8} cm^3 sec^{-1}
10^0
10^{-1}
1
2
3
4
5
20
40
E_H, keV

Fig. 4

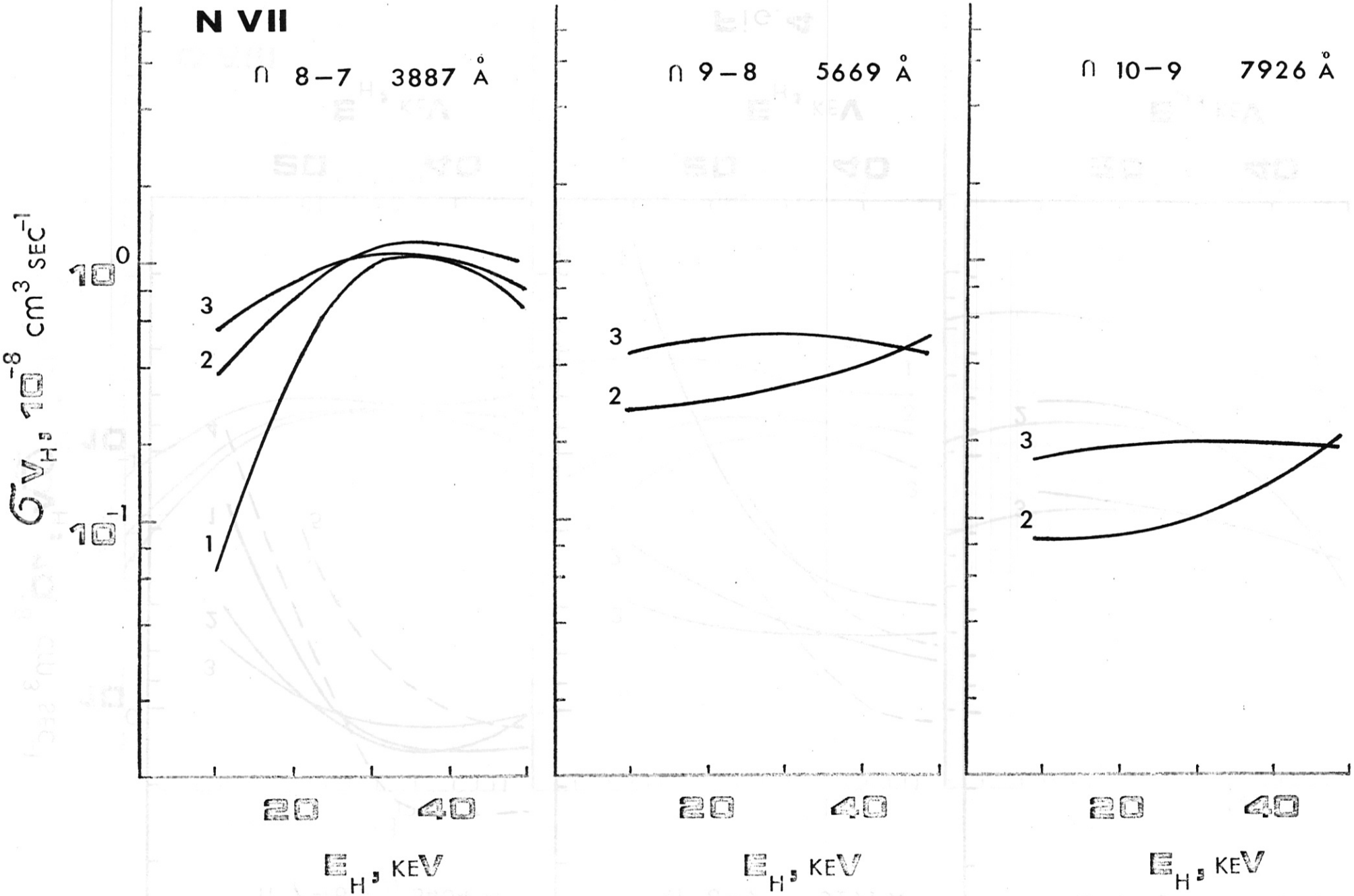
N VII
∩ 8–7 3887 Å
∩ 9–8 5669 Å
∩ 10–9 7926 Å
σv_H, 10^{-8} cm^3 SEC^{-1}
10^0
10^{-1}
1
2
3
20
40
E_H, KEV

Fig. 5

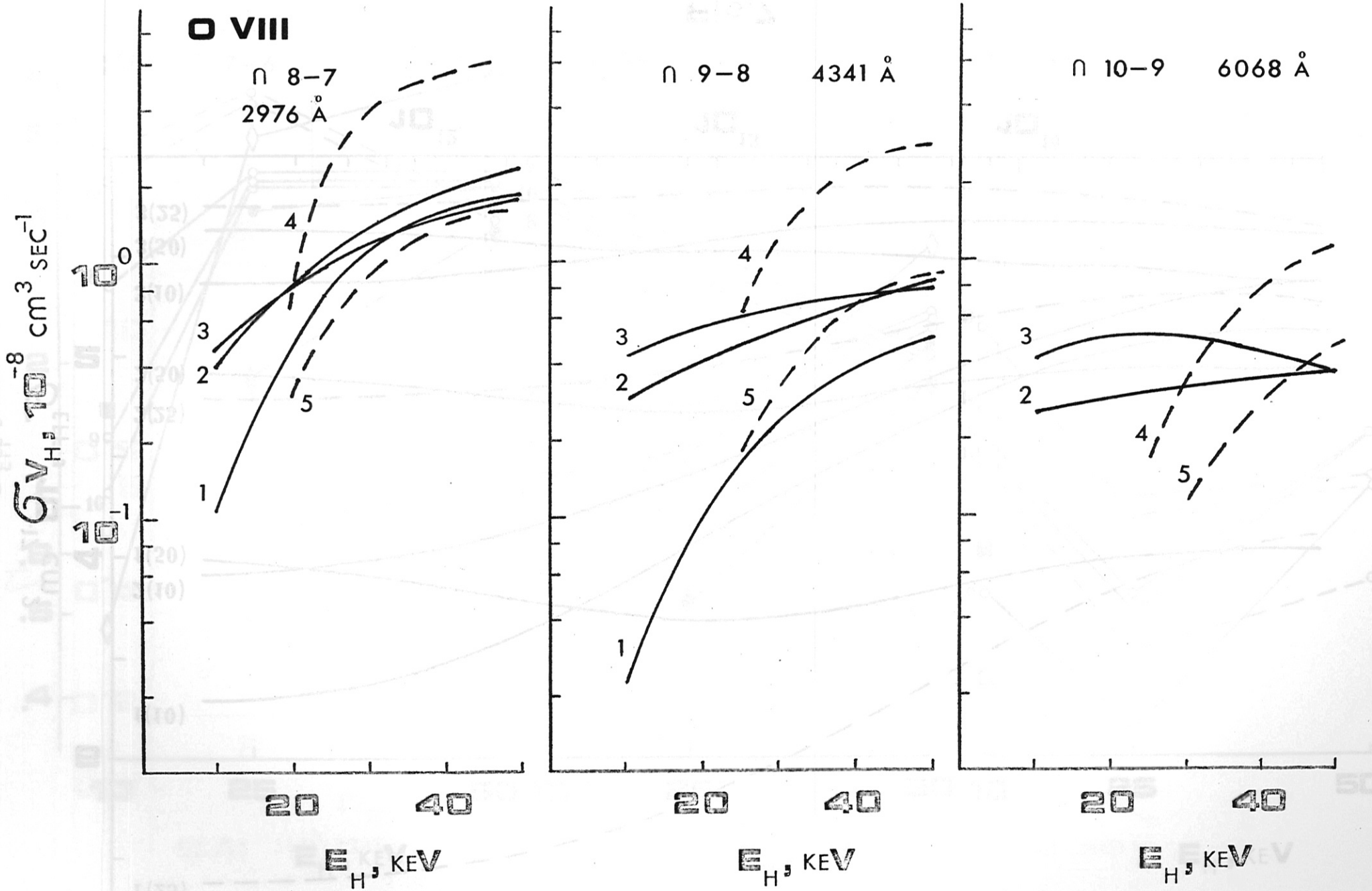
O VIII
∩ 8–7
2976 Å
∩ 9–8 4341 Å
∩ 10–9 6068 Å
σv_H, 10^{-8} cm^3 sec^{-1}
10^0
10^{-1}
1
2
3
4
5
20
40
E_H, KeV

Fig. 6

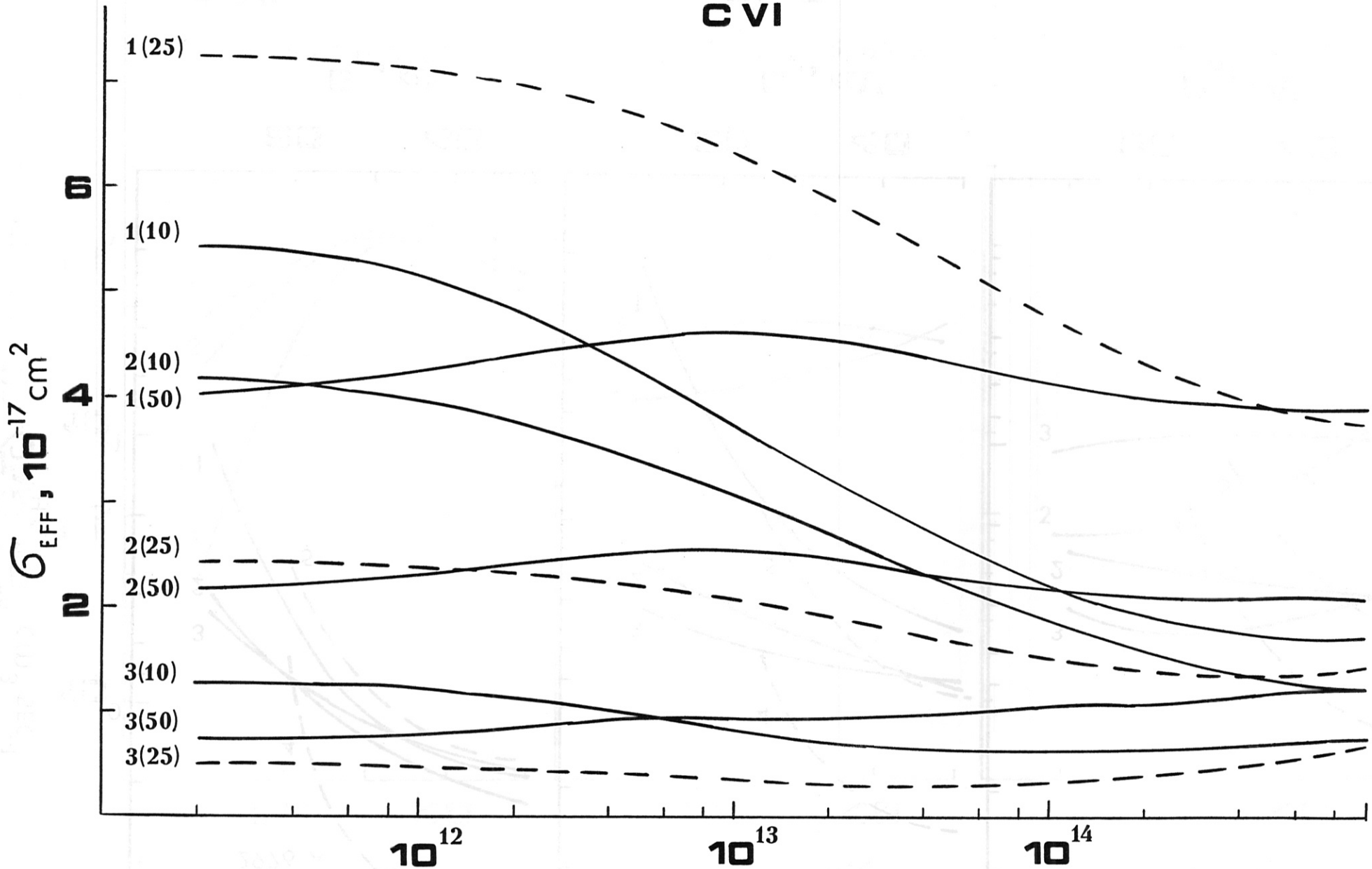
C VI
1(25)
1(10)
2(10)
1(50)
2(25)
2(50)
3(10)
3(50)
3(25)
6
4
2
σ_{EFF}, 10^{-17} cm^2
10^{12}
10^{13}
10^{14}

Fig.7

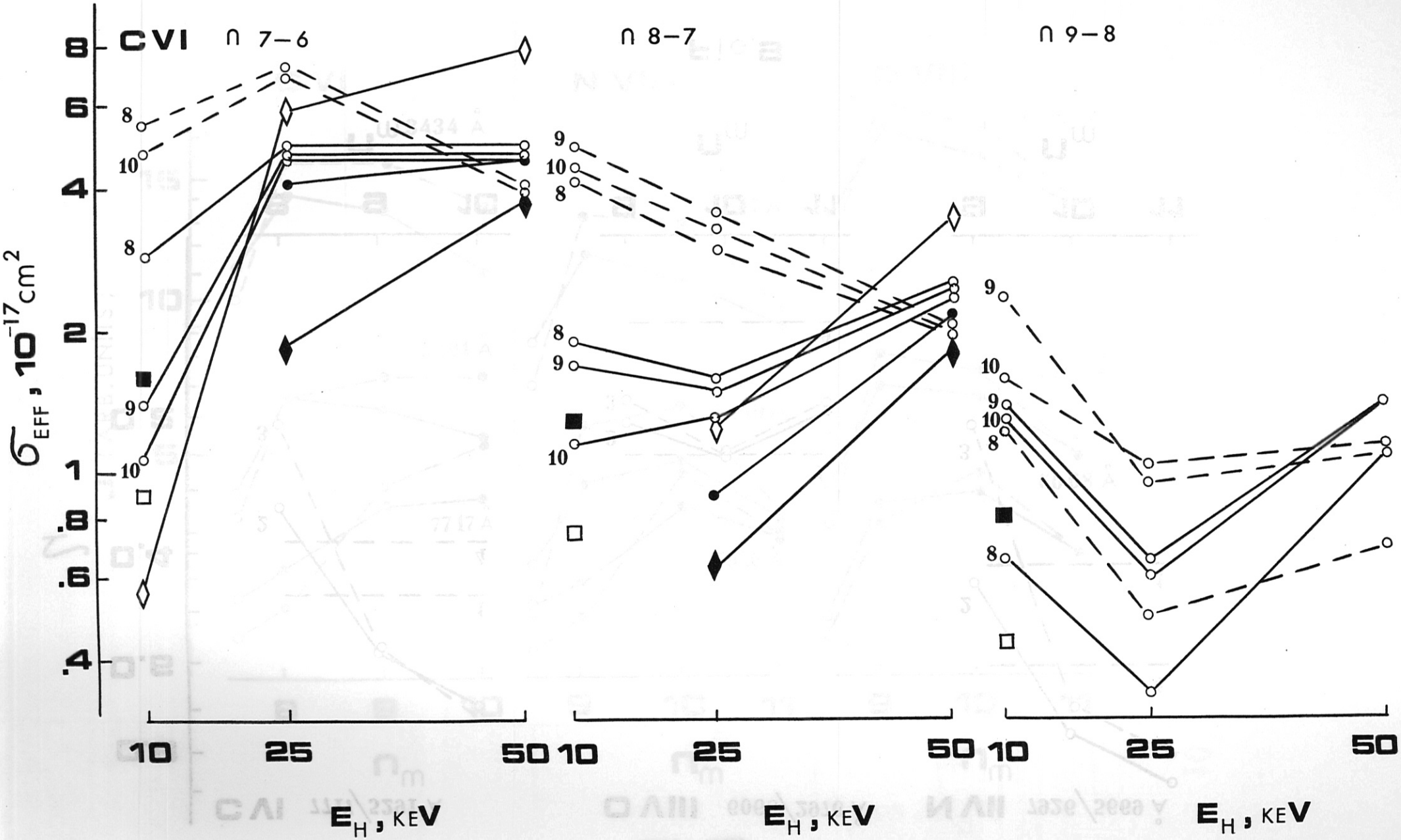

Fig. 8

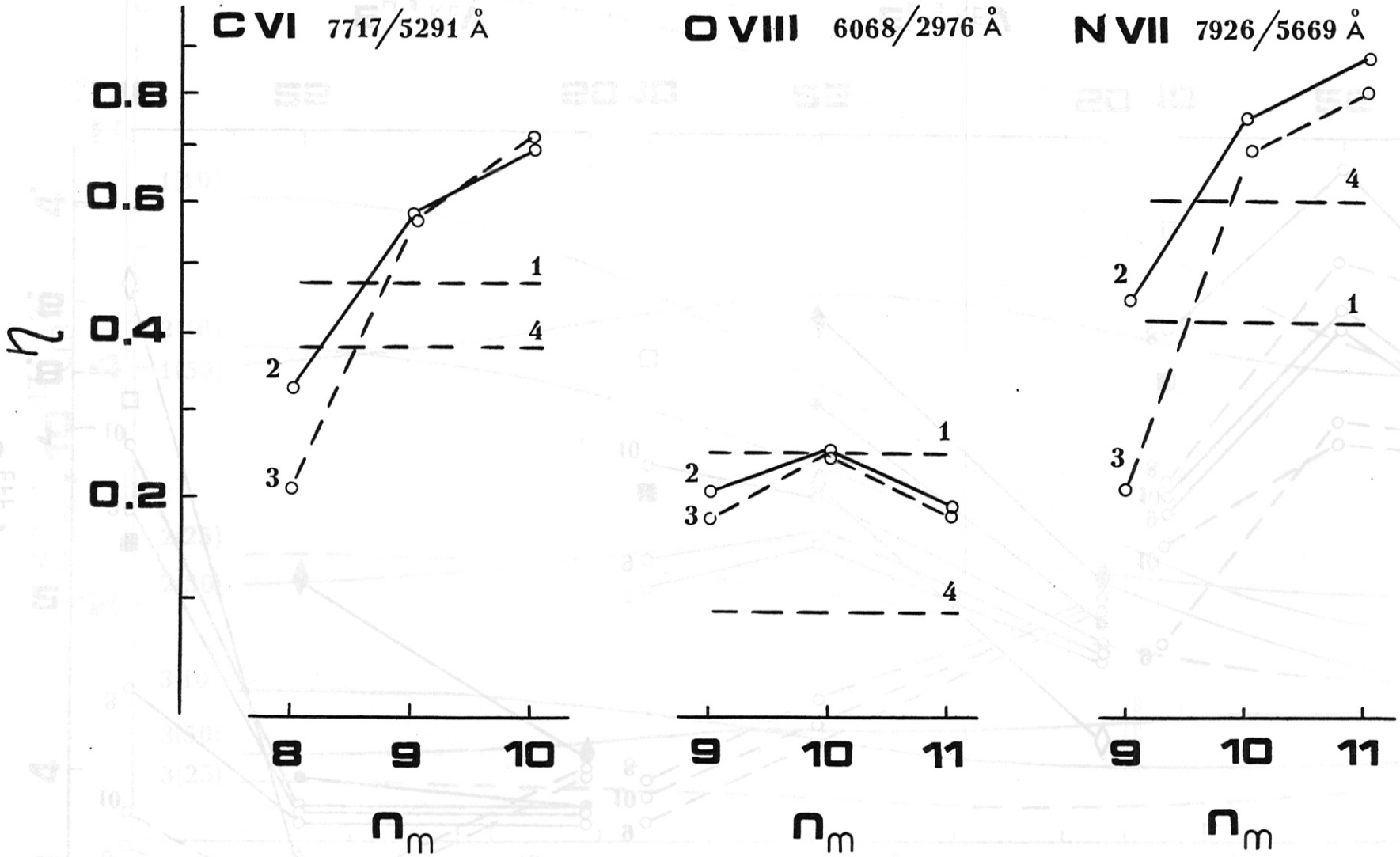
C VI 7717/5291 Å
O VIII 6068/2976 Å
N VII 7926/5669 Å
η
0.8
0.6
0.4
0.2
1
2
3
4
8
9
10
11
n_m

Fig. 9

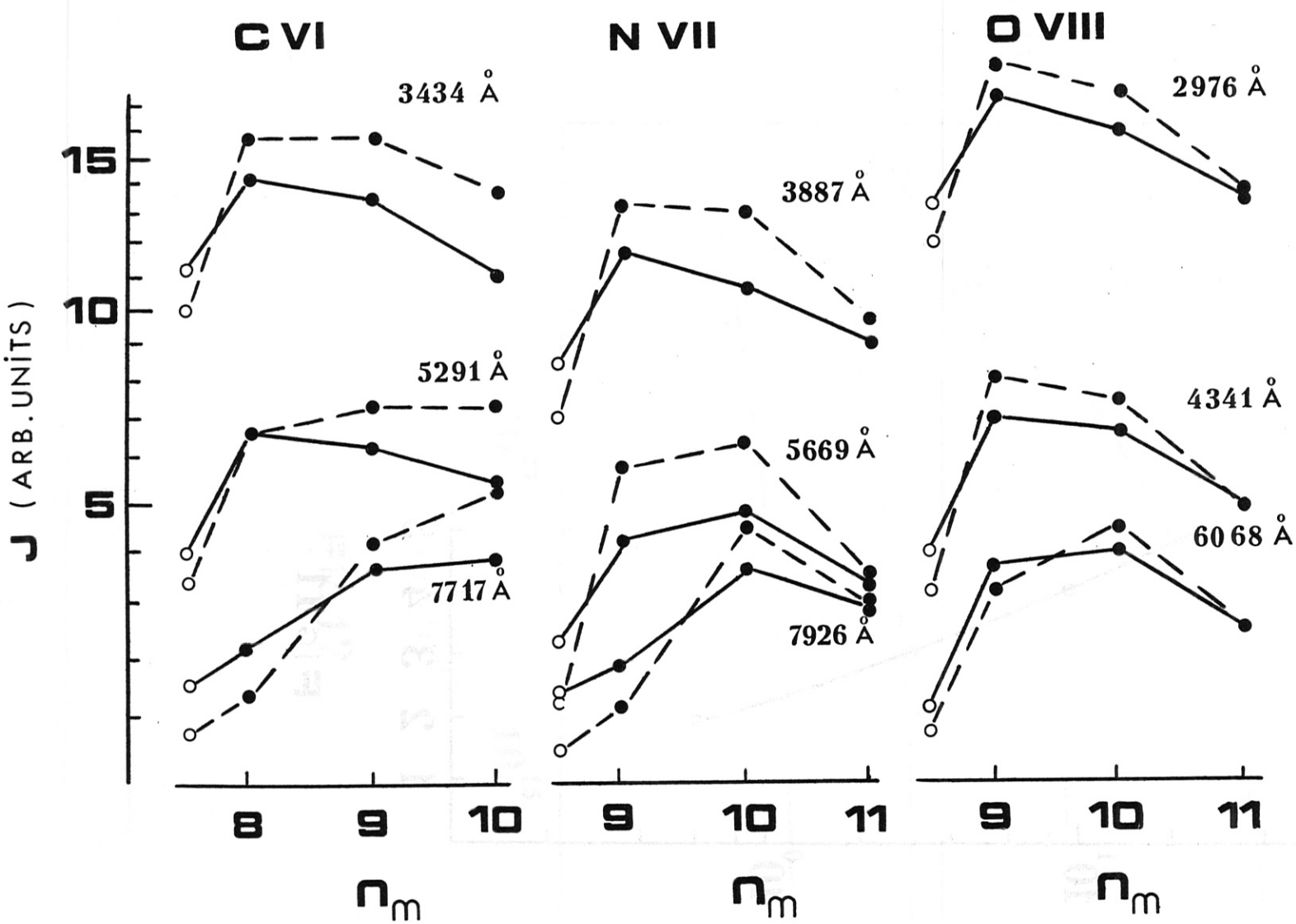
C VI
N VII
O VIII
3434 Å
5291 Å
7717 Å
3887 Å
5669 Å
7926 Å
2976 Å
4341 Å
6068 Å
J (ARB. UNITS)
15
10
5
8
9
10
9
10
11
9
10
11
n_m
n_m
n_m

Fig.10

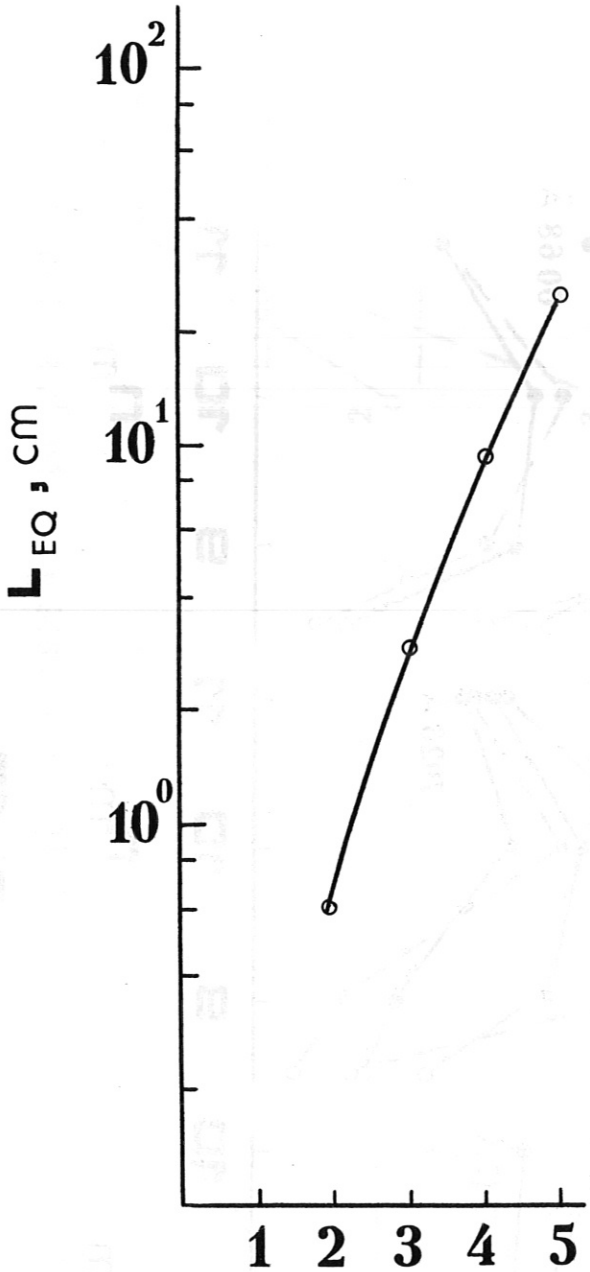

FIG. 11

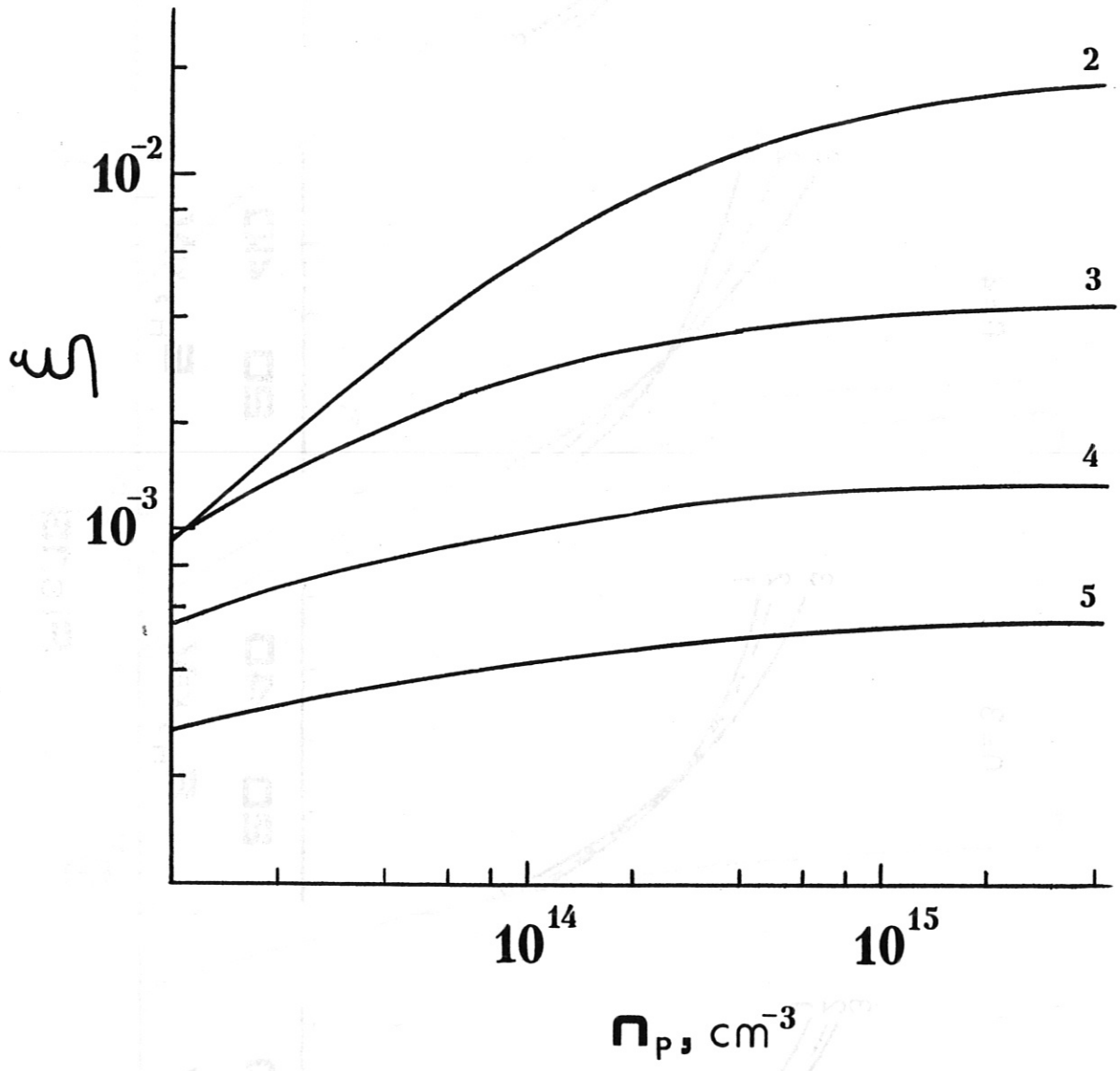

FIG. 12

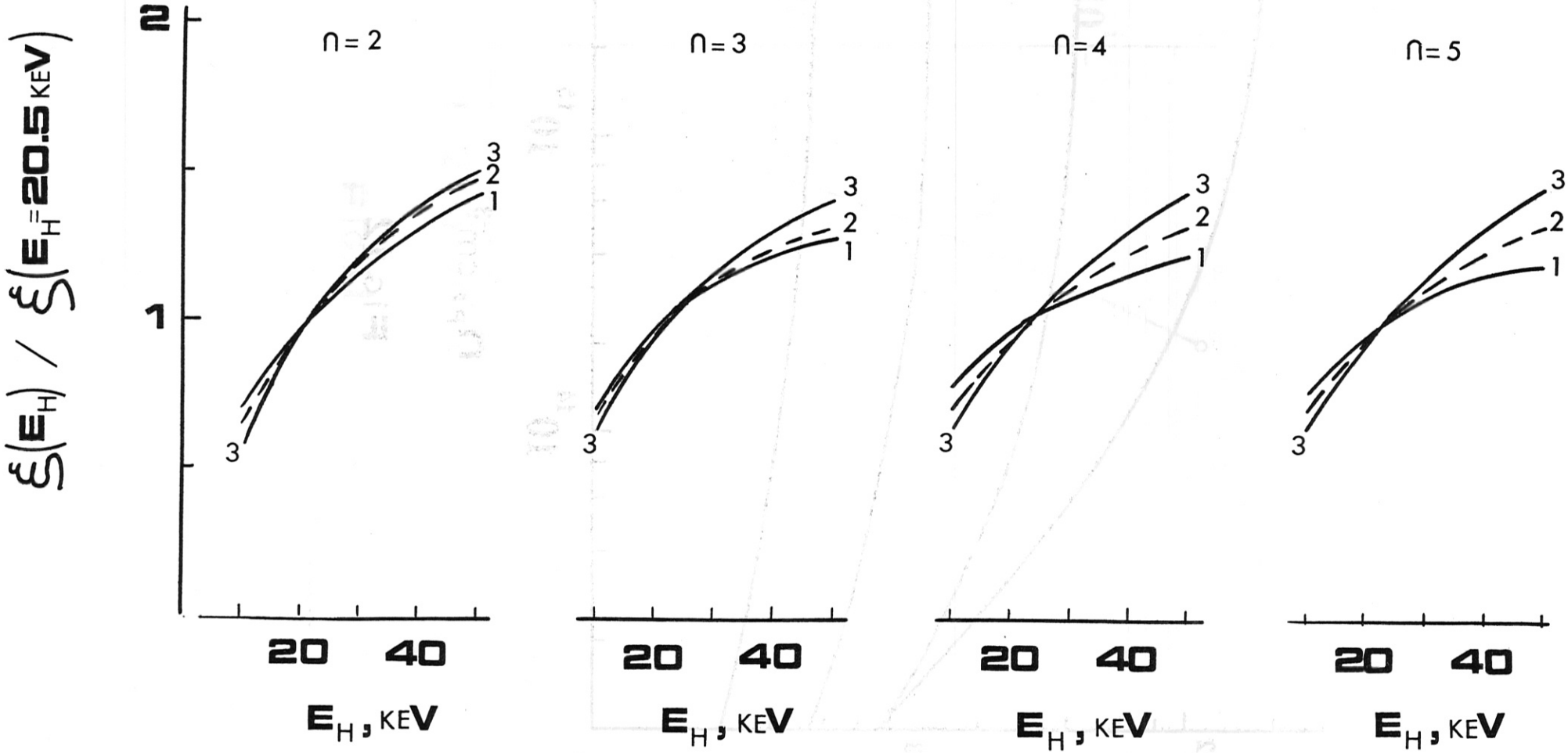

Fig.13

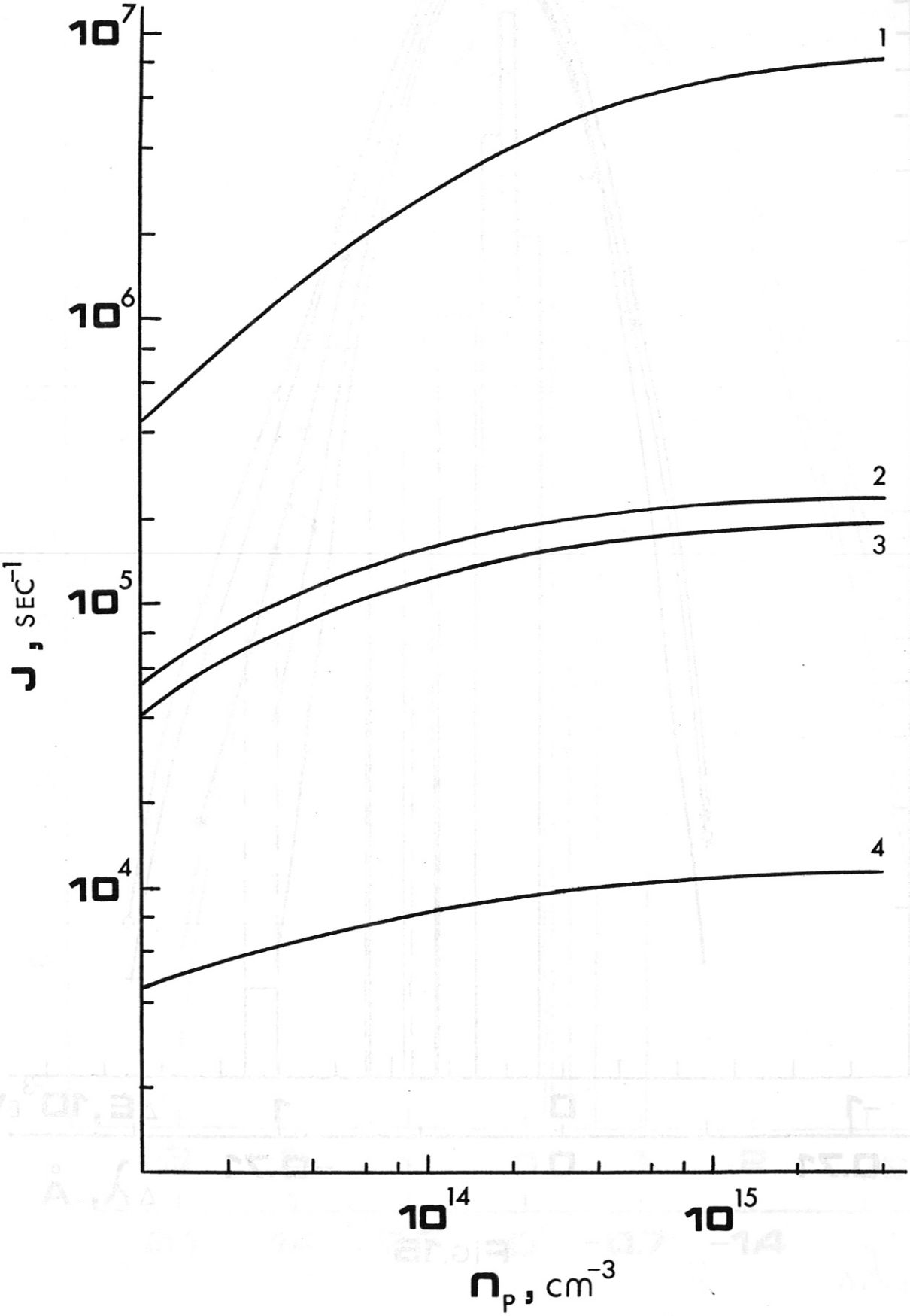

Fig.14

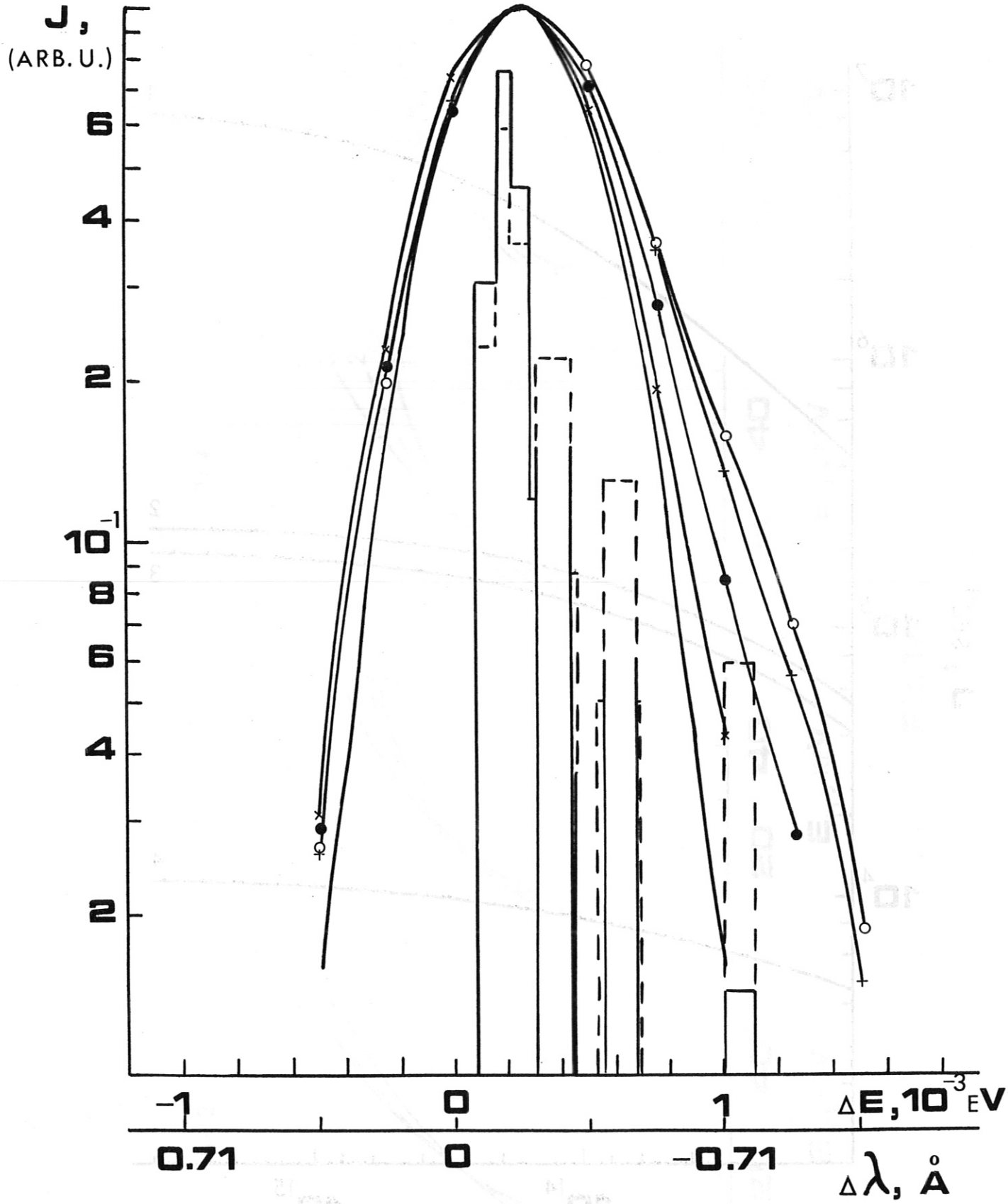

FIG. 15

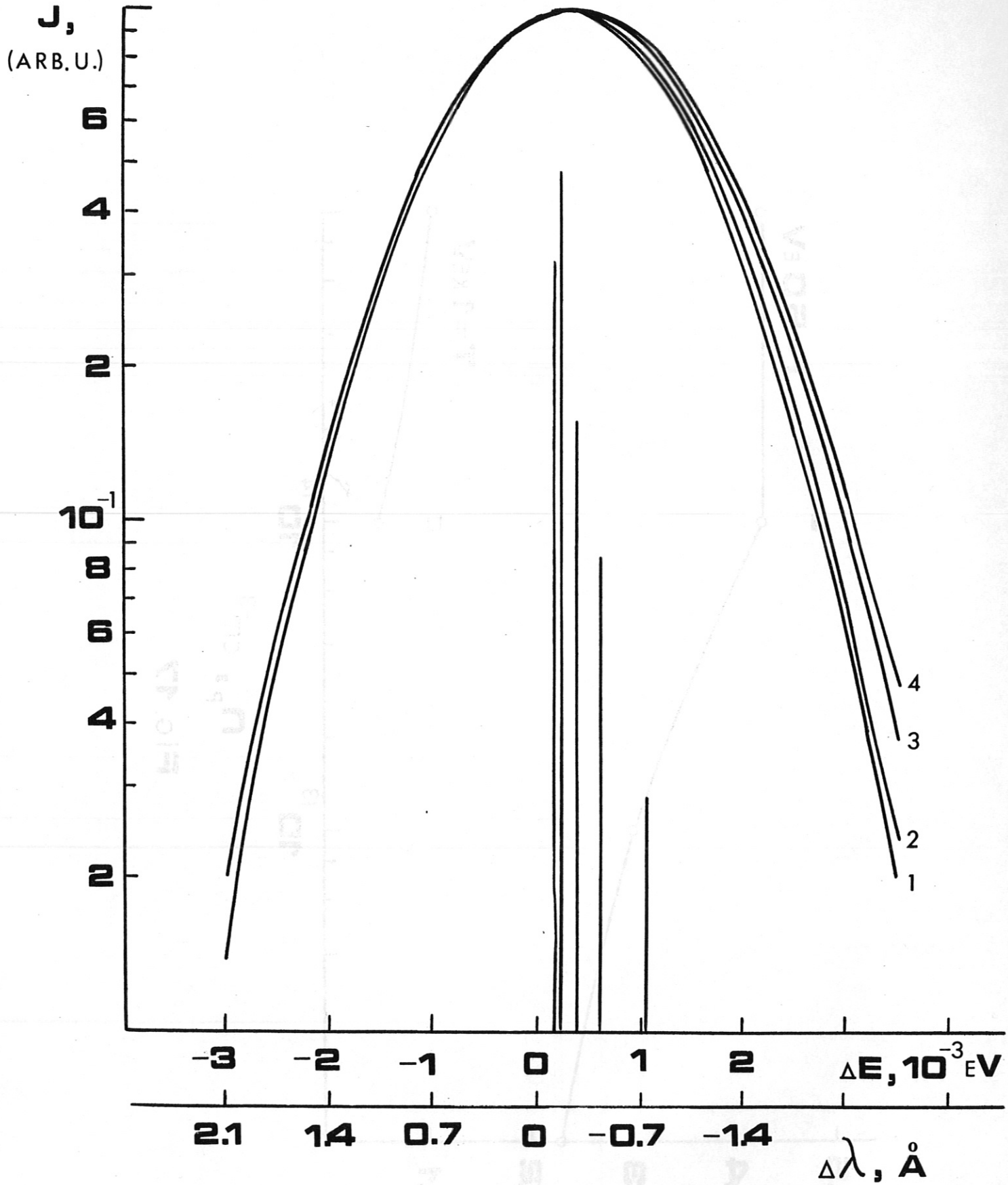

FIG.16

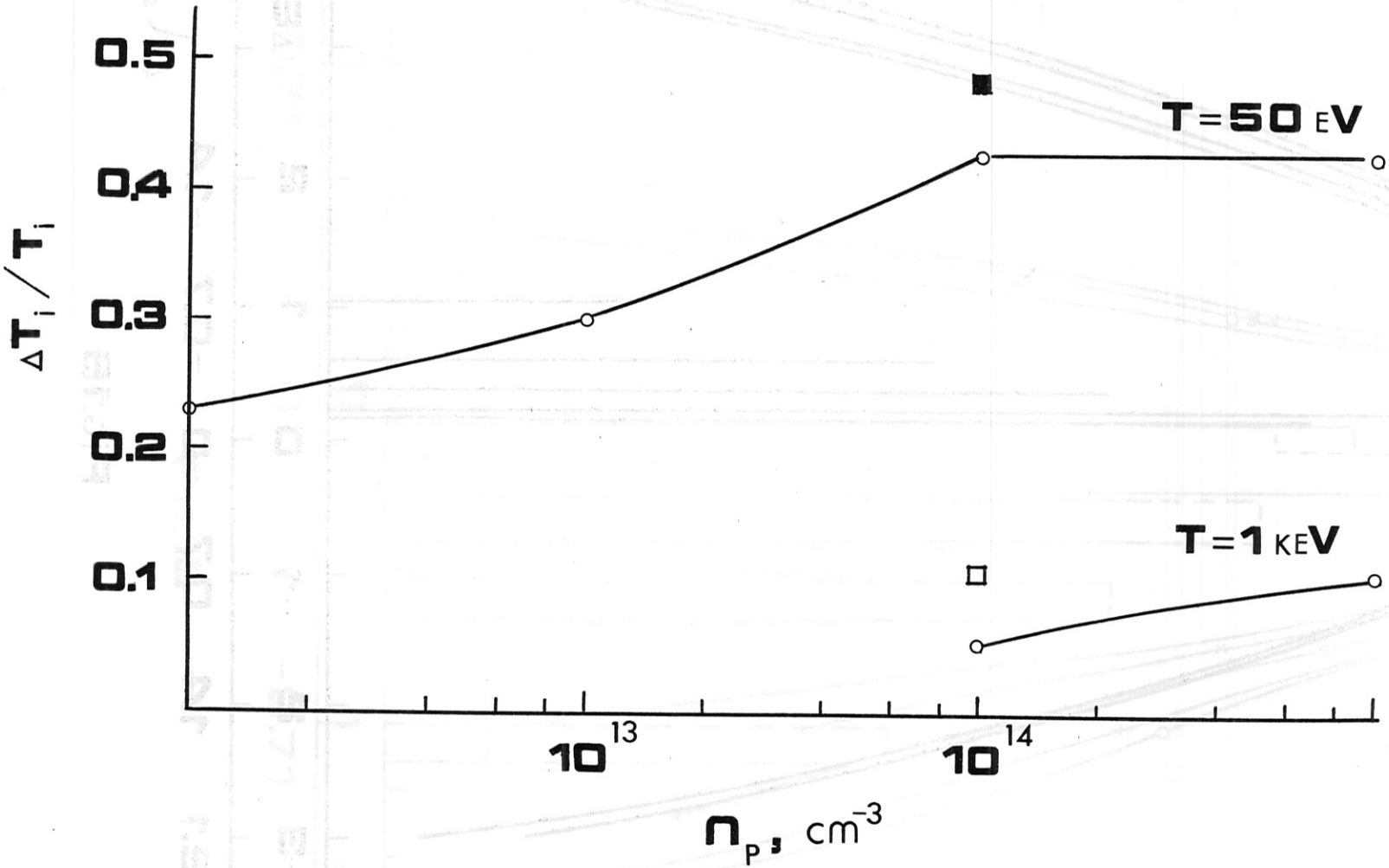

Fig. 17